In-Cylinder Aero-Thermal Simulation of Compression Ignition Engine: Using a Layering Meshing Approach

O. Moussa[1, 2†], A. Ketata[1], Z. Driss[1] and P. Coelho[3]

[1]*Laboratory of Electro-Mechanic Systems, National Engineering School of Sfax, University of Sfax, P.O. Box 1173, Road Soukra, 3038 Sfax, Tunisia*
[2]*Higher School of Sciences and Technologies of Hammam Sousse, University of Sousse, Lamine Abassi Street, 4011 Sousse, Tunisia*
[3]*Higher Technical Institute of Lisbon, DEM, University of Lisbon, Av. Rovisco Pais, 1049-001 Lisboa, Portugal*

†Corresponding Author Email: olfa.moussa@enis.tn

ABSTRACT

Three-dimensional flow simulations of the full cycle for four-valve direct-injection Diesel engine have been carried out with different meshes. The aim of the present study is to establish an extensive CFD investigation of in-cylinder aero-thermal flow of a direct-injection Diesel engine. The ICE-CFD solver is used to examine the unsteady behavior of a realistic engine configuration. Moreover, a layering approach and dynamic mesh model are adopted to generate the grid. The predicted radial velocity and swirl ratio for four different meshes are compared with Laser Doppler Velocimetry measurements and with numerical results from the literature. The comparison shows that the obtained results with the fine mesh present a good agreement with the experimental measurements along the compression phase and at the start of the expansion phase. In addition, these results are more accurate than the predicted results reported in the literature. Furthermore, CFD analysis is presented for the whole cylinder volume with regard to several parameters such as velocity field, swirling, tumble flow, pressure and temperature distributions. These results prove that in-cylinder CFD simulation gives reasonably accurate results that enable enhanced knowledge of the aero-thermal flow of full engine cycle.

Keywords: Compression ignition engine; Aero-thermal flow; Dynamic mesh; CFD simulation; Meshing effect.

NOMENCLATURE

B	bore	z	axial coordinate
d_b	bowl diameter		
h	specific enthalpy		
h'	specific enthalpy fluctuation	ε	turbulent dissipation rate
k	turbulent kinetic energy	μ	dynamic viscosity
n	engine speed	μ_{eff}	effective viscosity
P	static pressure	μ_t	turbulence viscosity
r	radial coordinate	ρ	fluid density
S	stroke	σ_k	turbulent prandtl numbers for k
SR	swirl ratio (dimensionless)		
T	temperature		
t	time		Abbreviations
TR	tumble ratio (dimensionless)	$ABDC$	At Bottom Dead Center
u	radial velocity	$aBDC$	after Bottom Dead Center
V	average velocity	$ATDC$	At Top Dead Center
V'	velocity fluctuation	$aTDC$	after Top Dead Center
Vp	mean piston speed	BDC	Bottom Dead center
Vi	the instant velocity component in the i direction	CFD	Computational fluid dynamics
		ICE	Internal Combustion Engine
Vj	the instant velocity component in the j direction	$ICEM$	Internal Combustion Engine Meshing
		TDC	Top Dead Centre
x	cartesian coordinate	CA	Crank Angle (degree)

1. INTRODUCTION

The knowledge of the thermo-fluid mechanics has an important role in the internal combustion engine (ICE) improvement. Recently, researchers have become increasingly interested in the in-cylinder fluid movement, heat transfer and combustion process which present important parameters that significantly affect the engine performances. Experimental studies have been performed by different methods such as the Laser Doppler Velocimetry (LDV) (Henriot *et al.* 1989; Payri *et al.* 1996; Kang *et al.* 1998 and Desantes *et al.* 2001) and the Particle Image Velocimetry (PIV) (Kampanis *et al.* 2001; Huang *et al.* 2005; Reeves *et al.* 1999 and O'Connor *et al.* 2013). These methods give high-quality results and provide detailed information on the velocity field inside the combustion chamber. However, these kinds of analysis techniques are costly and need an extensive time. That is why important growth of numerical techniques and computer capacities pushed the researchers to develop an efficient numerical approach in order to gain an accurate knowledge of the aerodynamic phenomena within the combustion chamber. In fact, there are different commercial codes such as ANSYS Fluent, Star-CD, and KIVA, or the specific codes based on C++, MATLAB and FORTRAN (Hedfi *et al.* 2014, 2016). Computational Fluid Dynamics (CFD) is an efficient tool for the engine simulation which has the advantage to reduce the cost and speed time. In this context, different numerical studies of the flow inside the combustion chamber have been carried out. On the one hand, the aerodynamic behavior at the level of the valves is frequently studied during the intake stroke (Mehta *et al.* 2001; Johan *et al.* 2001; Bilgin *et al.* 1999; Arcoumanis *et al.* 1982; Gazeaux *et al.* 2001). Gosman *et al.* (1984) and Yun (2001) performed a three-dimensional calculation of the air motion near the valves. In these studies, the intake and exhaust valves are considered as a unique moving area in which they obtained a difference between the flow model and the experimental data. Akar (2005) performed two-dimensional and three-dimensional simulations to study the effect of different valve gaps using the CFD solver ANSYS-Fluent. He reported that the position and length of the intake valve affect the flow structure. On the other hand, Payri *et al.* (2004) performed three-dimensional flow calculations of a four-valve direct-injection Diesel engine at the intake and compression strokes with different combustion chambers. They showed that the piston geometry presents insignificant effect on the in-cylinder flow during the intake stroke and the first part of compression stroke. In contrast, the shape of the bowl has a significant role near the Top Dead Center (TDC) and at the beginning of the expansion stroke.

Song *et al.* (2008) also explored the flow field characteristics in simplified piston bowls. They found that the piston geometries have a significant effect on the distribution of the cross section swirl ratio. Indeed, the tangential velocity profiles are nonlinear at the same position. Varol *et al.* (2010) studied the heat transfer and fluid flow inside a pent-roof type combustion chamber using the commercial code ANSYS-Fluent 12.0. They found that the flow structure and temperature distribution are affected by the shape of the combustion chamber and the revolution of the engine during the intake stroke. Moreover, Jayashankara and Ganesan (2010) studied the fuel injection timing and the intake pressure effect on the performance of a direct injection (DI) Diesel engine with a toroïdal combustion chamber configuration. They used the pre-processor GAMBIT for the creation of the entire computational domain and the commercial CFD code STAR-CD for the resolution of governing equations and post-processing the results. The calculated results were validated with experimental data from the literature. They indicated that the predicted results of radial velocity, swirl ratio and turbulent intensity using the CFD give good agreements with experiments. Barbouchi and Bessrour (2009) investigated the turbulent and time-dependent flow in the cylinder whole. Indeed, a numerical calculation based on the finite element method by means of powerful simulation code CASTEM of CEA was carried out. They obtained a reasonable agreement with the experimental data. Hadj Kacem *et al.* (2016) studied experimentally the influence of the hydrogen enrichment on the engine performance and the exhaust emissions. Then, they developed three-dimensional simulations using the SolidWorks Flow Simulation code for investigating the effect of the LPG-hydrogen blends (0, 10 and 20% of H2) on one spark ignition Engine. They showed that the hydrogen enrichment has a good impact on the in-cylinder flow characteristics and engine performance. Kim *et al.* (2009) studied numerically the performance of two-different Exhaust Gas Recirculation (EGR) systems in order to reduce the pollutants emissions and improve the combustion behavior. They performed a three-dimensional combustion calculation using the commercial code STAR-CD and the standard k-ε turbulence model. Indeed, mixing features, EGR gases distribution and admitted air were compared under different operating conditions. Sushma and Jagadeesha (2013) performed a three-dimensional simulation of the in-cylinder flow in compression ignition engine. CATIA-V3 was used to design the geometry and Hypermesh-10.0 as a meshing tool. By the end, the data was exported to the solver ANSYS-Fluent 13.0 for completing the mesh. They confirmed that the design of the inlet manifold configuration and the piston geometry is very important in IC-Engine. But, its computational cost was still too high for the engine design. From these studies, it is clear that the modern IC-Engines are characterized by intricate geometry, moving piston, canted valves, complex form of the cylinder head and the piston bowls. For these systems, the mesh generation presents one of complex tasks in the CFD simulation.

The main objectives in this present paper are to present and demonstrate a new meshing approach of the computational domain of the internal combustion engine. Indeed, the mesh independence test is carried in order to done the accurate minimum mesh cells size and provide good results. A 3D axisymmetric geometry of internal combustion engine equipped

with a toroïdal piston bowl is adopted to compute the cold flow simulation. The standard k-ε turbulence model is used to solve the governing equations. A comparison in term of non-dimensional radial velocity and swirl ratio is done to validate the proposed meshing method. Then, an analysis of the average velocity, in-cylinder pressure and temperature is presented without reaction from the fuel injection. This analysis gives a clear insight on real conditions in combustion chamber.

2. ENGINE GEOMETRY

In the present work, a single cylinder diesel Direct Injection (DI) engine has been used with a toroïdal piston bowl. The engine speed is set equal to 2000 rpm. The engine characteristics are listed in Table 1. The 3D model of the engine geometry is illustrated in figure 1. It was established by using the Pre-Processor design modeler of Internal Combustion Engine ICE-CFD analysis systems tools. In the ICE-CFD analysis system, the computational domain must include the combustion chamber with the inlet and exhaust valves to obtain a realistic calculation (Ansys 2015). Indeed, the combustion chamber of these simulations is a straight-roof type counting two-inlets and two-exhaust ports. In addition, the piston bowl has a toroïdal form.
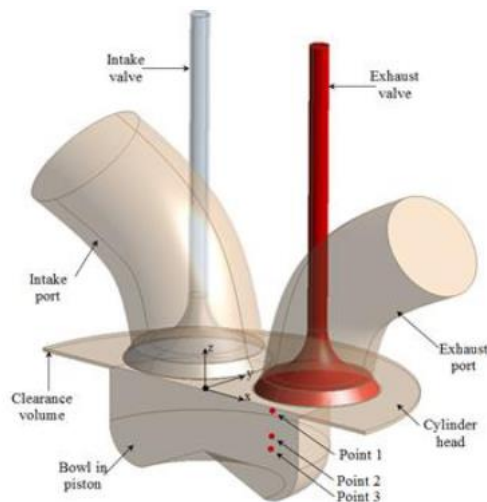
Fig. 1. Computational domain.

3. CFD PROCESS

It is well known that experimental tests are very expensive and it is difficult to visualize the different in-cylinder physical phenomena. That is why, CFD tools are mostly used to develop the ICE technology (Sukegawa *et al*. 2003). Besides, we have used ICE-CFD analysis system to investigate the aero-thermal phenomena inside the combustion chamber for cold flow simulation. ICE solver advantages consist of computational domain decomposition into different zones. In fact, this stage facilitates the meshing setup and allows the application of the moving mesh method in different zones. It can also perform an unsteady in-cylinder simulation.

Table 1 Engine characteristics

Fuel	Diesel
Technology	Direct Injection (DI)
Number of cylinder	one
Bore (B)	130 mm
Stroke (S)	150 mm
Bowl diameter (Db)	76 mm
Bowl depth (db)	29 mm
Average engine speed	2000 rpm
Compression ration	17.1
Intake valve open	9° BTDC
intake valve close	242° ATDC
Exhaust valve open	137° BTDC
Exhaust valve close	10° ATDC

3.1 Meshing and Boundary Conditions

The generation of the engine geometry grid with the classical meshing tools is very complex task on account of the complex geometry which consists of the piston and valves movement. Then, the O-grid blocking is not possible therefore the grid refinement is not feasible. For this reason, a new meshing approach, based on the ICEM-CFD software, was performed to rectify the difficulty faced with the classical meshing tools and to present the utilities of the required grid refinement. The ICEM-CFD software presents important advantages which can generate O-gird, L-grid and V-grid needed for certain complex form of geometry. Also, it can refine the grid with control on the distribution of mesh and possibility to check and ameliorate the grid quality. In this proposed approach, all the engine parameters such as the shape of the piston crown and the cylinder head, the number, the size and the position of the valves, then the squish and clearance length should be considered in advance. In fact, the imported engine geometry is decomposed into different volume before meshing and each volume is meshed separately as presented in figure 2. The meshing strategy is adopted by considering in advance all the geometric features of the engine such as valves piston crown and cylinder head shape, squish and clearance length. The layering mesh approach is adopted in this stage to simulate easily the piston and valve motions in the IC-engine simulation. Table 2 summarizes the mesh information of the considered zones. Based on the new meshing methods, four different grids are generated in order to study the mesh resolution influence on flow simulations results. They are designed in zero crank angle position at the TDC. For the first case, the mesh cell is finer only at the valve seat which it is critical to accurately control the opening and the closing of valve and the grid is coarser than the other parts (figure 3.a). Then, a progressive local refinement of the mesh zones has been done allowing thereby the generation of three meshes of the cases b, c, and d as presented in figures 3.b, 3.c and 3.d. In these cases, the mesh cell is more

refining at the cylinder combustion chamber and the valve seat. The piston bowl and valves are provided with dynamic mesh. For this reason, it is meshed with hexahedral cell. However, the static zones are meshed with tetrahedral cell to reduce computational time. Indeed, these three meshes are only differenced by the refinement degree at the aforementioned zones. The total number of the mesh cells is ranged from 107520 to 2778849 mesh cell at the TDC. The characteristics of the considered grids generated in this work are summarized in table 3. It is important to determine the right total number of mesh cell to ensure that it is neither too low until causing high deviation from the right result, nor too high that can cause long computational time. For the validation of the developed simulations, the experimental data of Payri *et al.* (2004) has been used. In order to reproduce the realistic conditions of the engine, some boundary conditions have been considered. Indeed, a constant pressure is assumed at the inlet and the exhaust ports. The walls are considered adiabatic. In addition, constant temperature is set on the cylinder and piston walls and an initial turbulent intensity of 5% of the average flow has been considered.

Table 2 Fluid zones and mesh requirement details

N°	Fluid zone	Mesh requirements
1	Fluid-valveID-port	Any mesh
2	Fluid-valveID-ib (inboard)	Mesh with at least one layer at the top
3	Fluid-valveID-vlayer	layered mesh
4	Fluid-ch-lower	Layered mesh
5	Fluid-ch-upper	Any mesh
6	Fluid-ch-valveID	Layered mesh
7	Fluid-piston	Any mesh

3.2 Mathematical Equations

ANSYS 17.0 ICE solver is used in this work to perform 3D cold flow simulations inside the combustion chamber during four strokes of the engine cycle. The Navier-Stokes equations are solved based on the classical finite volume method using this commercial software. Particularity, we have used the pressure correction and PISO algorithm (Driss *et al.* 2012). Standard k-ε turbulence model is adopted for the flow simulation (Dillies *et al.* 1998 and Moussa *et al.* 2017). The temporal discretization is implicit with regard to time depending on stroke stage. The second order upwind scheme is employed to discretize the momentum, energy and turbulence equations. The radiation mode is neglected compared to other heat transfer modes. The simulation begins at the Top Dead Center (TDC) and ends at 50° after the Bottom Dead Center (aBDC) for an engine speed equal to 2000 rpm. The

mathematical model of the compressible, unsteady and turbulent in-cylinder flow is computed with regard to continuity, momentum, energy and turbulence equations (Bilgin, 1999 and Jameel *et al.* 2009).
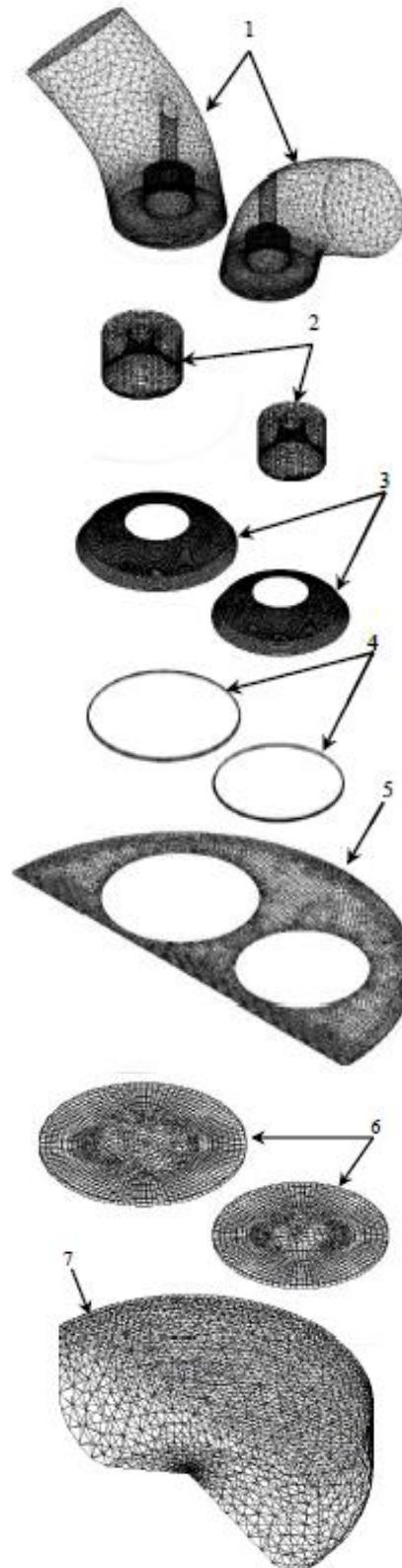
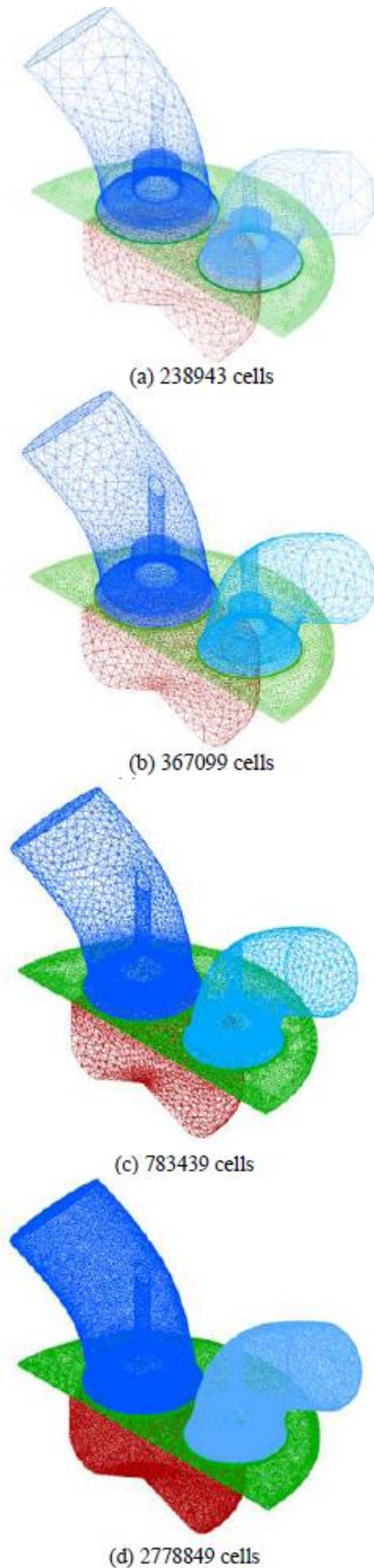**Fig. 2. Fluid zone and mesh boundary details.**

(a) 238943 cells

(b) 367099 cells

(c) 783439 cells

(d) 2778849 cells

Fig. 3. 3D views of the grids independence.

Table 3 Meshing grid characteristics

Mesh	Total nodes number		Total cells number	
	ATDC	ABDC	ATDC	ABDC
Coarse (a)	107520	350241	238943	596218
Medium (b)	163461	683209	367099	843556
Fine (c)	330116	1669595	783439	2222467
Very fine (d)	916198	3820545	2778849	6782144

Mass, momentum conservation, and energy equations can be written as:

$$\frac{\partial \rho}{\partial t} + \frac{\partial}{\partial x_j}(\rho V_j) = 0 \tag{1}$$

$$\frac{\partial}{\partial t}(\rho V_j) + \frac{\partial}{\partial x_j}(\rho V_i V_j) = -\frac{\partial p}{\partial x_i}$$
$$+ \frac{\partial}{\partial x_j}(\mu[(\frac{\partial V_i}{\partial x_j} + \frac{\partial V_j}{\partial x_i}) - \frac{2}{3}\delta_{ij}(\frac{\partial V_k}{\partial x_k})]) \tag{2}$$

$$\frac{\partial(\rho h)}{\partial t} + \frac{\partial}{\partial x_j}(\rho V_j h) = \frac{\partial}{\partial x_j}(\frac{\lambda}{c_p}\frac{\partial h}{\partial x_j} - \overline{\rho h' V_j'}) \tag{3}$$

Where:

ρ is the density and Vj is the component of the instant velocity in the j direction (j = 1, 2, 3).

$-\rho \overline{h' V_j'}$ define the correlation terms between the velocity fluctuation.

h is the enthalpy, which is defined by the specific enthalpy hk for each species presented by:

$$h = \sum_{k=1}^{n} Y_k h_k \tag{4}$$

The standard k-ε turbulence model is based on the work of Launder and Spalding (1986). The equations for the turbulent kinetic energy and its dissipation rate are solved by assuming that the flow type is fully turbulent and the m olecular viscosity. These two equations can be written as:

$$\frac{\partial(\rho\varepsilon)}{\partial t} + \frac{\partial(\rho V_j\varepsilon)}{\partial x_j} = \frac{\partial}{\partial x_j}[(\mu_{eff} + \frac{\mu_t}{\sigma_k})\frac{\partial\varepsilon}{\partial x_j}]$$
$$+ C_{\varepsilon 1}\frac{\varepsilon}{k}P_k - C_{\varepsilon 2}\rho\frac{\varepsilon^2}{k} \tag{5}$$

In the standard k-ε turbulence model, the turbulent viscosity μt can be defined according to the Prandtl–Kolmogorov:

$$\mu_t = \rho C_\mu \frac{k^2}{\varepsilon} \tag{6}$$

The effective viscosity is written as follows:

$$\mu_{eff} = \mu_t + \mu \tag{7}$$

The constants of the standard k-ε turbulence model are presented in table 4.

Table 4 Constants of the standard k-ε turbulence model

| c_μ	σ_k	c_{ε_1}	c_{ε_2}	σ_ε
0.09	1	1.44	1.92	1.3

4. MESHING OPTIMIZATION AND MODEL VALIDATION

In this part, results of aero-thermal simulation of compression ignition engine are presented and validated. Firstly, the meshing independence choice is studied. Then, they are compared to the experimental data of Payri *et al.* (1996). In addition, the new meshing approach is adopted in this study and its results are compared with the traditional meshing method of the gambit software (Payri *et al.* 2004).

4.1 Mesh Independence Test

The numerical results of the normalized radial velocity within the combustion chamber, obtained at three points placed under the cylinder head of 4 mm, 12 mm, 16 mm respectively in the points a, b and c in figure 1 are performed with four different mesh cell number. Hence, they are compared to the LDV experimental results of Payri *et al.* (1996) in order to check the grid independence. The air flow profile inside the combustion chamber linearly evolved with the engine speed (Sushma *et al.* 2013 and Sukegawa *et al.* 2003). So, to obtain an accurate comparison of the numerical results, it is suitable to normalize the radial velocity by the mean piston speed Vp.

Figure 4 depicts the non-dimensional radial velocity as a function of the crank angle in the three points placed under the cylinder head for the different meshes. For the coarse grid consisting of 107528 nodes at the TDC, a large difference has been observed in the simulation and for the three considered positions. At the last time of the compression stroke and at a distance of 4mm from the cylinder head, a good comparison with the test data is obtained by the two refined meshes consisting of 330116 nodes and 916198 nodes. In these conditions, an average error of 8% has been recorded during the compression phase and near the TDC between the predictions and measurements results. After that, it varies from 10% up to 15% at the points defined between z = -4 mm and z = -12 mm. In contrast, the difference decreases at z = -16 mm from the cylinder head to 5% along the compression and exhaust strokes. It has been noted that a centripetal flow has been observed when the piston approaches to the TDC. This flow moves towards the bowl beginning from the values of velocity close zero to reach a highest value. Up to the TDC, the piston moves up and presents a centripetal motion of the flow, which is maintained at the beginning of the

expansion stroke. From these results, a good agreement between numerical and experimental results is found with the tow refining grids and it confirms the validity of the numerical model. Taking into account the limitation of the computational resources used in this study as well as the resolution time for the solution convergence, the refined mesh consisting of 783439 unstructured hexahedral and tetrahedral cells at the TDC seems to be the best choice for predicting accurately the diesel engine performance.


(a) z = -4 mm

(b) z = -12 mm

(c) z = -16 mm
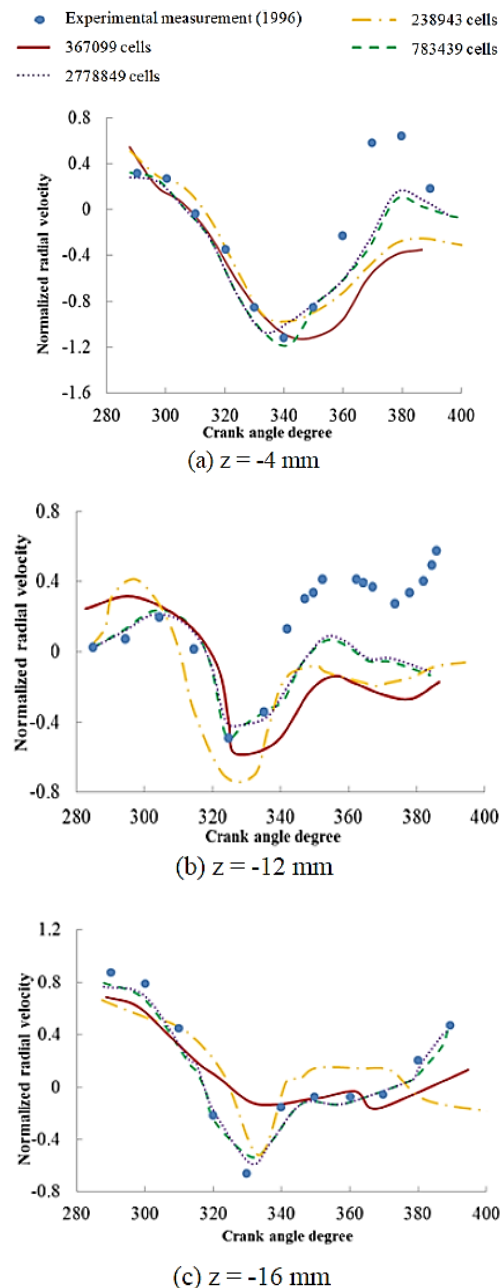
Fig. 4. Non-dimensional radial velocity profiles.

4.2 Model Validation

In order to present the effect of the layering meshing approach involved in this study on the flow calculation, the numerical results from the selected

grid of 783439 cells and 330116 nodes at the TDC have been compared to both numerical and experimental results of Payri *et al.* (2004). Figure 5 depicts this comparison in terms of the normalized radial velocity and the swirl ratio against the crank angle at a distance of -4 mm from the cylinder head. From figure 5.a, it has been observed that the error of the predicted normalized velocity from the developed method to test data is less than 4% after the TDC and 7% at the TDC. These results are significantly lower than that presented by Payri *et al.* (2004). In fact, the average errors of their predicted results got from the old meshing method by means of the Gambit software. This observation led to a significant deviation of the normalized radial velocity with the test data since the calculated average error is between 9% and 15%, during the compression stroke and at the first stage of expansion stroke. From figure 5.b, it has been shown that the developed meshing method yielded to better accuracy of the predicted swirl ratio during the two first engine strokes compared to the method used by Payri *et al.* (2004). In fact, the maximum error of the predicted swirl ratio to the test data is about 3%. This value is lower than the predicted results founded by Payri *et al.*(2004), which is about 8%. According to these results, it can be deduced that the proposed meshing method allows a better accuracy of the numerical results, especially for the local characteristics of the fluid flow inside the combustion chamber.
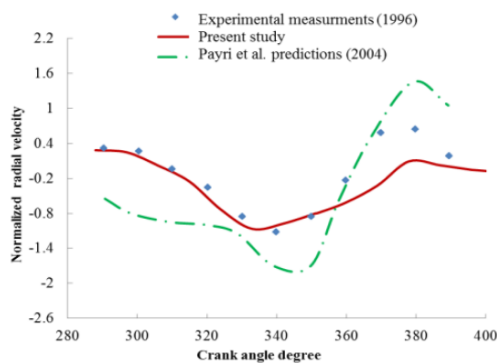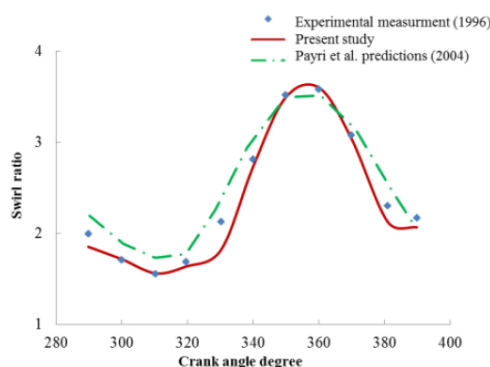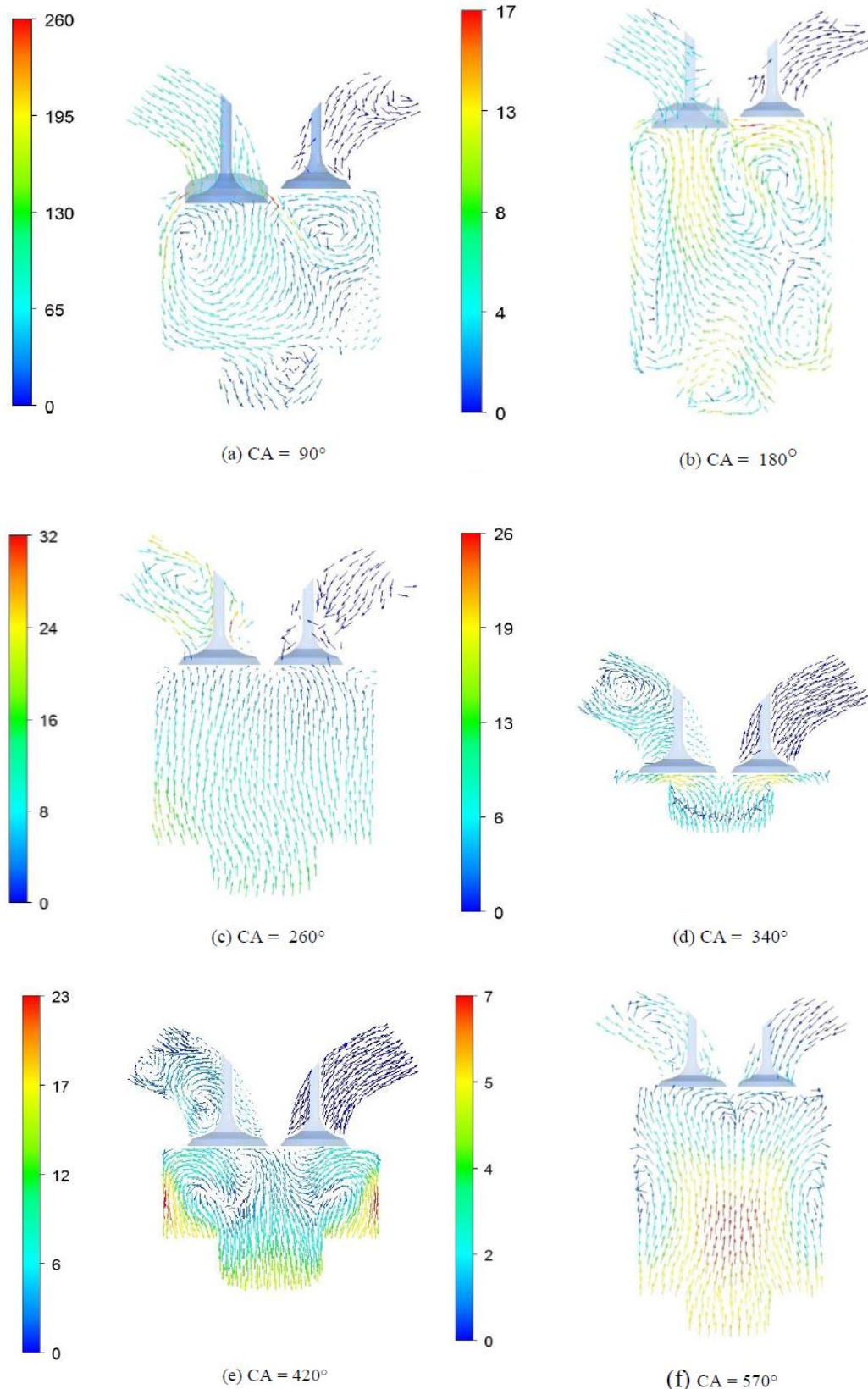
5. NUMERICAL RESULTS AND DISCUSSION

In this section, a 3D flow simulation was studied in order to identify and understand the in-cylinder aero-thermal phenomena. Several parameters, such as velocity field, swirling and tumble ratio profile, in-cylinder pressure and temperature distribution, were obtained against of the crank angle in different planes of the chamber. In addition, the z-pressure and z-temperature variation are characterized with regard to the z-position inside the cylinder. Figure 6 presents the computational domain with the planes of measurements of the different parameters as cited above.

5.1 Average Velocity

Figure 7 depicts the average velocity field along the axial cross-section for different crank angle values. At the beginning of the induction phase, the jet effect is localized in the valve gap where the maximum values of the average velocity are observed. This fact is caused by the small gap at periphery of the intake valve. In addition, the small space between the cylinder head and the piston surface impose an important effect on the intake flow distribution. In fact, this flow is not developed in the others direction. Then, the displacement of the piston from the TDC towards the BDC generates a conical intake flow as a function of the crank angles (Figure 7.a). In this phase, it is clear that the cylinder volume occupied by the air increases and the important interaction between the intake flow and the cylinder walls produces two-recirculation zones in the cylinder periphery. Hence, it accumulates and impinges on the piston surface where a third vortex is created in the piston bowl. For a higher crank angle, the piston speed is almost constant and the intake valves are totally open; since it is the end of the induction stroke (Figure 7.b). In this stage, the inlet velocity value of the intake flow decreases and becomes much lower than the value at the first stage of the intake stroke.

(a) Non-dimensional radial velocity

(b) Swirl ratio

Fig. 5. Comparison with LDV measurement of Payri and its predictions (2004) at z = - 4 mm.
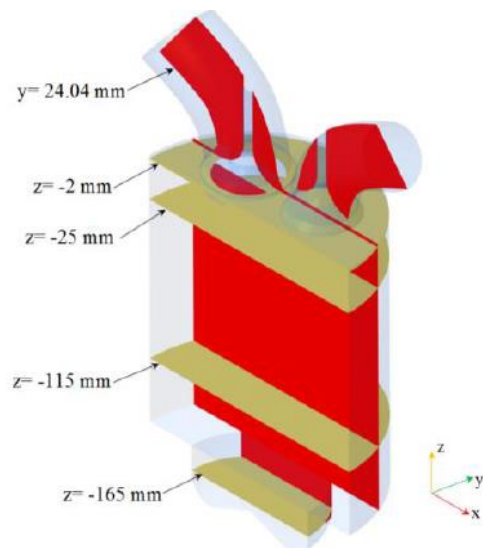
Fig. 6. Visualization planes.

(a) CA = 90°

(b) CA = 180°

(c) CA = 260°

(d) CA = 340°

(e) CA = 420°

(f) CA = 570°

Fig. 7. Mean velocity field in mid-section during the engine cycle.

In contrast, the circulation zone is stabilized at the same region. The compression stroke starts just after the induction stroke when the piston moves upwards.

However, the real compression process begins with the closure of the intake valves. In fact, in our calculation, the total closure of the intake valves is at

a crank angle of 240° bTDC. At the beginning of this stage, the toroïdal vortexes generated at the intake stroke are conserved and the flow velocity becomes approximately homogeneous inside the cylinder and the piston bowl. These toroïdal vortexes disappear progressively as the piston moves towards the cylinder head and squeeze the charge from a large volume to a small volume with increasing of the crank angle. The forced upwards flow impinges the cylinder head (Figure 7.c). When the piston is approaching to the TDC, a strong interaction between the impinging flow into the piston and the impinging flow into the surface of the valve and the walls is observed inside the small volume of the combustion chamber. As results, the velocity magnitude under the cylinder head is equal to V=26 m.s-1. Globally, the expansion stroke is initiated after the ignition process when the valves are closed. However, in our simulation we are interested in the cold flow without combustion reaction. The studied cold flow is used to analyze the basic characteristics of the internal engine geometry. At this stage, the hot compression flow forces the piston and displaces it to the BDC. Strong toroïdal vortexes are generated inside the cylinder, and propagate near the cylinder head and close to the cylinder vertical walls at the end of this stroke. Furthermore, the maximum value of the velocity is observed near the bottom side of the lateral walls, and it is equal to V=23 m.s-1 at the beginning of the expansion stroke (Figure 7.e). This value decreases and is localized in the cylinder center at the end of this stroke (Figure 7.f). Globally, the maximum velocity value is lower than that obtained at the beginning crank angle for the intake and the compression strokes.

5.2 Swirling flow and Tumble Ratio

The fluid flow is characterized by two movements: the tangential and the axial rotational movements defined, respectively, by the swirl and tumble ratios (Huang *et al.* 2005). These movements can be evaluated according to several parameters. In fact, the tangential rotary movement analysis is quantified by the swirl ratio (SR):

$$SR = \frac{v(\theta)}{\frac{2\pi n}{60}r} \qquad (8)$$

The tumble ratio is due to the squish motion when the piston approaches to the TDC. It can be considered as a ratio of the average angular velocity of the vortices at a certain crank angle to the engine speed:

$$TR = \frac{\sum_{i=1}^{N}(\frac{\partial w}{\partial z} - \frac{\partial u}{\partial x})_i}{2n\omega} \qquad (9)$$

Where

$(\frac{\partial w}{\partial z} - \frac{\partial u}{\partial x})$ are the vortices for tumble ratio and ω is the crank shaft angular speed.

Figure 8 shows the variation of the swirl ratio within the combustion chamber against the crank angle degree. Swirl ratio is considered as one of the important parameter used to quantify the fluid motion inside the cylinder. According to these results, it has been observed that the swirl ratio variation change from positive to negative values or vice versa during the admission stroke. Indeed, it presents a little fluctuation at the beginning of the intake stroke from 0 CAD to 20 CAD. This fact can be explained by the small opening of the intake valve at this interval where it produces a high velocity in the intake flow around the intake valve seat. After that, the swirl ratio decreases until a minimum value equal to -0.60 and gradually increases until the maximum lift position of the intake valve. After that, it decreases again at the end of the admission stroke. The swirl ratio is peaked approximately at the middle of the intake stroke which is equal to 0.72.
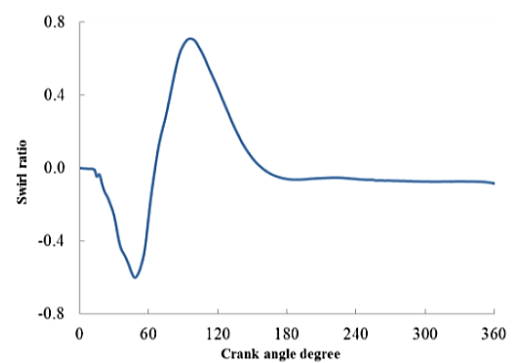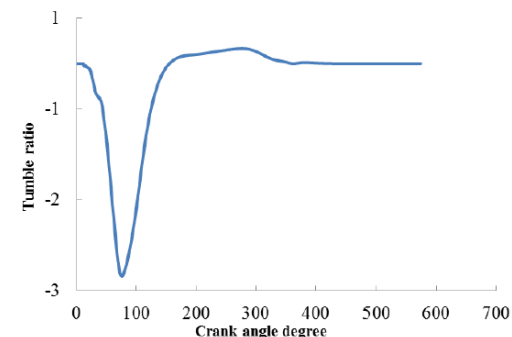

Fig. 8. Evolution of the swirl ratio.

Fig. 9. Variation of the tumble ratio.

In figure 9, the tumble ratio inside the cylinder with respect to the crank angle during the intake and compression stroke is displayed. From these results, it can be seen that, the tumble ratio variation gradually decreases from the TDC until the middle of the admission stroke. The minimum value in this interval reaches -2.4 which it refers to the change in the overall tumble flow pattern due to low-pressure zones. Then, the tumble ratio variation increases from the middle stage of the intake stroke to the middle stage of the compression stroke. Hence, it is peaked where the piston displaces from the BDC until 280 CAD which it is equal to 0.4. However, the tumble ratio decreases again when the piston moves another time to the TDC. As consequence, the large variations of the swirl ratio and the tumble ratio show the overall evolution of the airflow in its direction with the Crank angle. This fact is due to the change
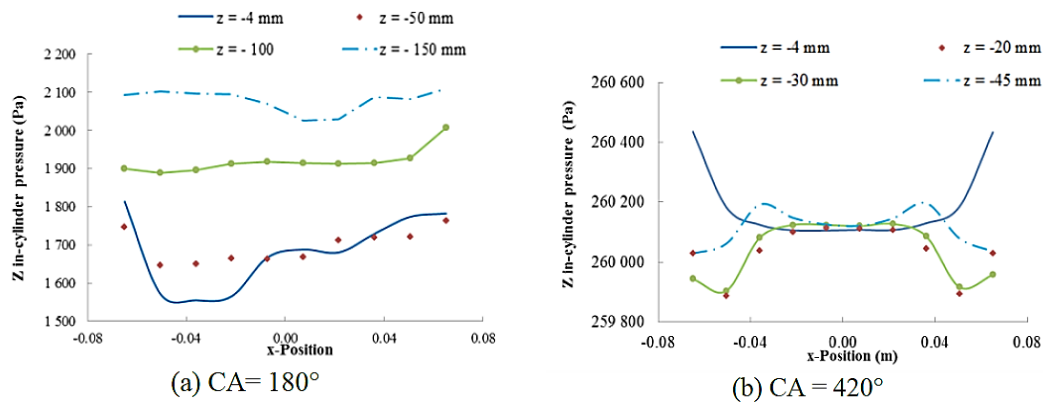
(a) CA= 180°   (b) CA = 420°

Fig. 10. In-cylinder pressure profiles.

in the direction of the piston.movement during suction and compression strokes and to the modification in the piston speed against the crank angle.

5.3 In-Cylinder Pressure

The in-cylinder pressure is another parameter studied to accurately comprehend the flow motion behavior inside the combustion chamber. Figure 10 shows the pressure variation through the end of the intake stroke and expansion stroke. This distribution is plotted with regard to the different axial positions defined by z = - 4 mm, z = -20 mm, z= -30 mm, z = -45 mm, z = - 50 mm, z = -100 mm and z = -150 mm from the cylinder head. At the end of the induction stroke, it was observed that for all the z-positions, the in-cylinder pressure is globally taken as uniform with x-position as presented in figure 10.a. For example for z = -100 mm, the average value of the in-cylinder pressure is equal about P = 1920 Pa and for z = 150 mm, it reaches to P = 2100 Pa. The change of the in-cylinder pressure magnitude is observed only at the inlet valve placement near the cylinder head at z = -4 mm. This fact is explained by the opening of the intake valve. Indeed, it has been observed also that the maximum value of the pressure is noted at z-positions more distant from the cylinder head. For 420° aTDC, when the intake and exhaust valves are closed, the pressure variation is approximately uniform with x for all the z-positions. In contrast, it presents a change near the wall of the cylinder. Furthermore, the distribution of the in-cylinder pressure is illustrated in figure 11 at the end of the intake stroke in different transverse planes with a scale size equal to 0.3. From these results, it has been noted that the high-pressure distribution is around the wall of the cylinder for all the z-position. The minimum value is around the intake valves seat at z = -2 mm as shown in figure 11.a, while the pressure distribution increases for the z-positions further the cylinder head. Therefore, the maximum value is obtained in the piston bowl for z= -165 mm as presented in figure 11.d.
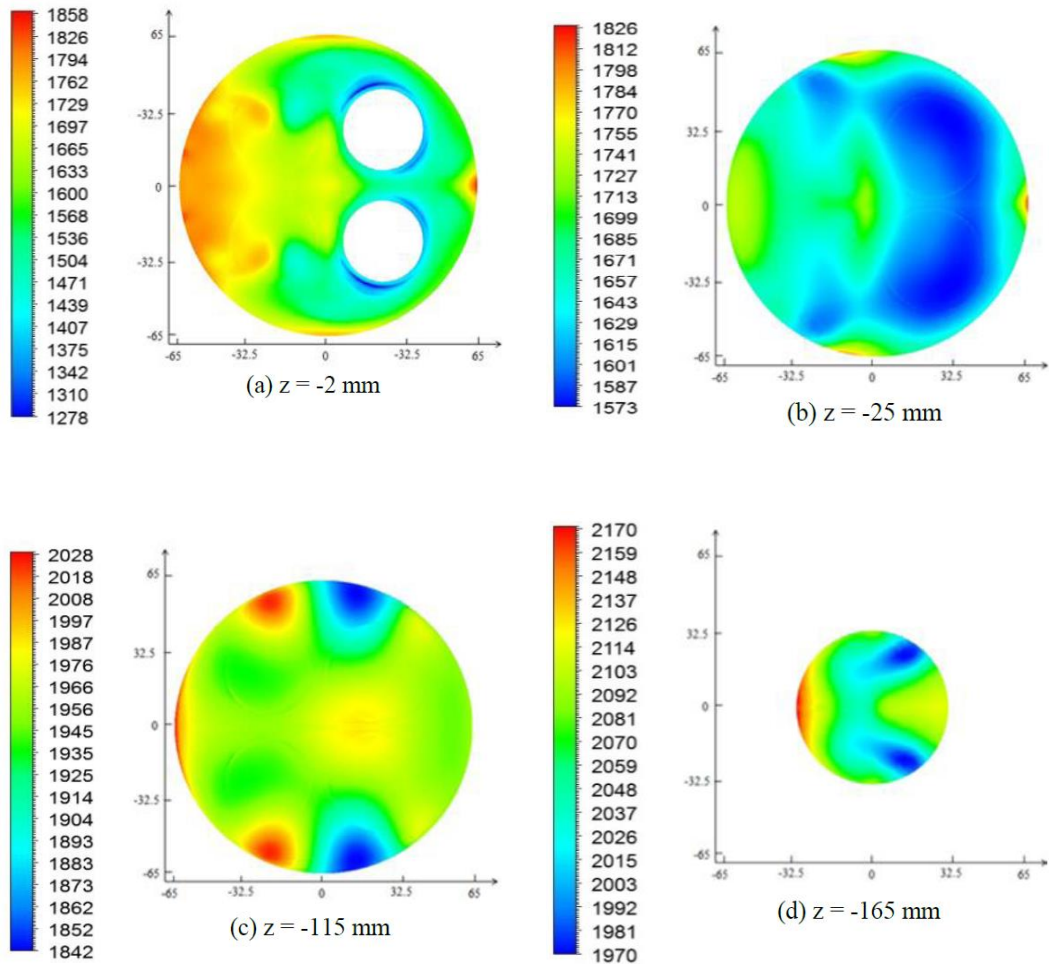
5.4 Temperature

The temperature variation with respect to the different lines of measurements at the end of the

induction stroke and the middle of expansion stroke is plotted in figure 12. As shown in figure 12.a, when the piston is at the top dead center, the temperature variation is minimum for x= -0.065 m and x = 0.065 m. In fact, these two positions correspond to the sides limit of the cylinder wall. In these conditions, the temperature is maximum from x= -0.049 m until x= 0.049 for all the z-positions. Near the cylinder head, the temperature variation presents a little increase around the valve intake seat. Then, it increases rapidly to attain the maximum value. From figure 12.b, at the middle of the expansion stroke, the profiles of temperature present the same behavior for all the lines of the measurement. The minimum value of the temperature is noticed at the sides of the cylinder head and the maximum value is obtained from x= -0.049 m until x= 0.049 m.

In figure 13, the distribution of the temperature is presented at the end of the intake stroke for the different planes defined in figure 6. According to these results, it was confirmed that the distribution of the temperature admits a highest values inside the cylinder and lower at the cylinder wall for each z-positions. In addition, the maximum values is observed in the piston bowl for z= -165 mm (figure 13.d). However, the minimum values are obtained near the cylinder head.

To properly show the temperature development, figure 14 presents the distribution of the temperature at a cross-section passing from the valves axis at a radial distance of 34 mm during the engine cycle. From this figure, it has been noted that from the middle of the intake stroke until the end of the compression stroke, the temperature variation increases with the increase of the crank angle. In contrast, it decreases during the expansion and exhaust strokes (Figures 14.e and 14.f). The highest temperature has been observed within the cylinder especially in the piston bowl for all the crank angles. However, the maximum value is obtained at a crank angle degree equal to 340°, when the piston is near the TDC, and it reaches 770 K as shown in figure 14.d. This fact is due to the decrease of the combustion chamber volume and the increase of the in-cylinder pressure. Consequently, the internal energy and the thermal agitation increase.
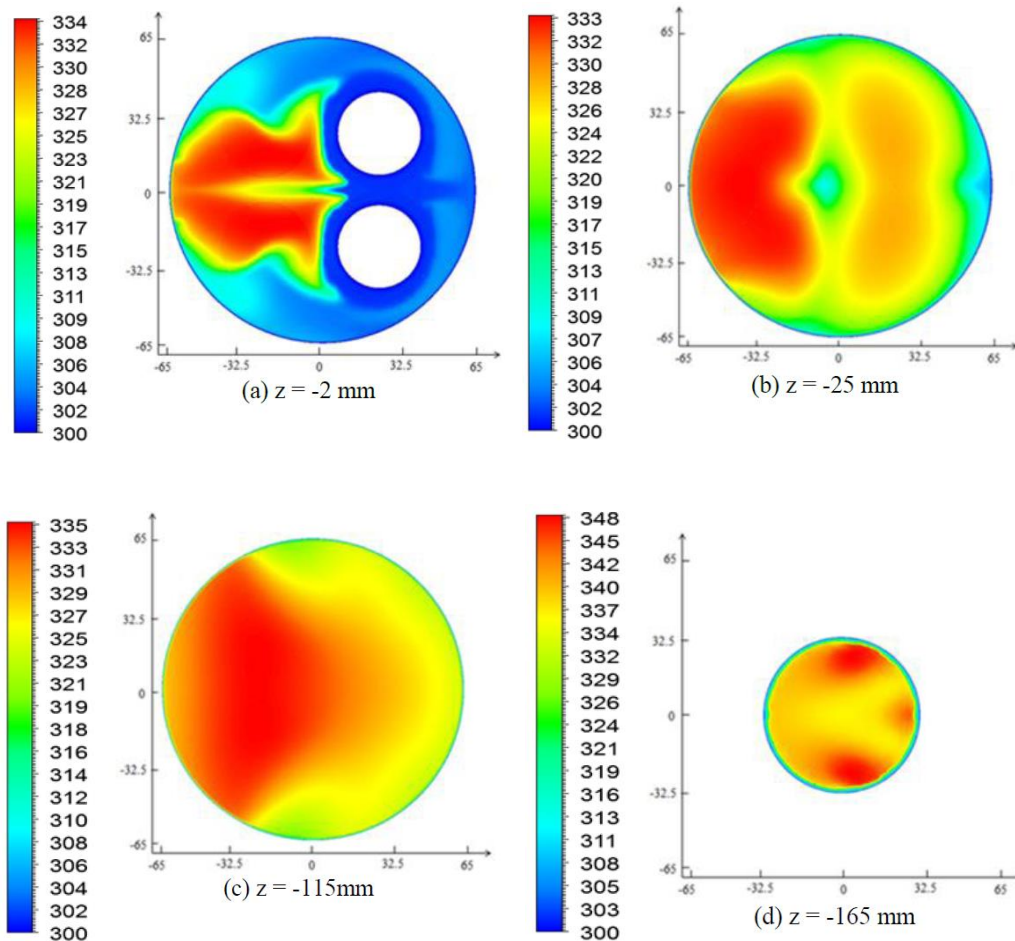
Fig. 11. Pressure distribution in the transverse planes at 180 CAD.
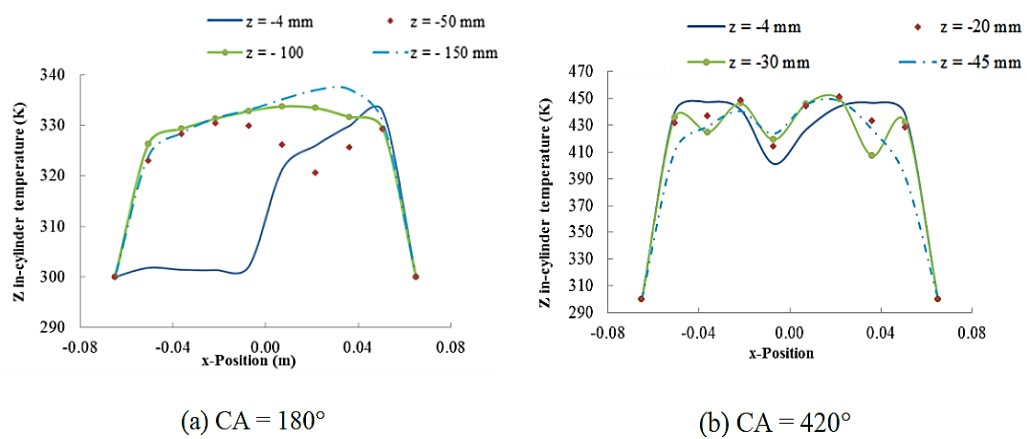
(a) CA = 180°   (b) CA = 420°

Fig. 12. Z in-cylinder temperature profiles.

(a) z = -2 mm

(b) z = -25 mm

(c) z = -115mm

(d) z = -165 mm

Fig. 13. temperature distribution in transvers planes at 180 CAD.

5. CONCLUSION

3D numerical analysis using a new meshing approach was carried out in order to understand properly the in-cylinder flow motion in the internal combustion engine. Firstly, four different mesh cells number were developed to determine the accurate minimum total number of the grid cells which can provide accurate results from the simulation. Then, the obtained results from the selected mesh cells was compared in term of non-dimensional radial velocity and swirl ratio to both the numerical and experimental test of anterior results to present the advantages of the new meshing approach than the traditional meshing tools. The standard k-ε turbulence model is used to solve the governing equations for unsteady, compressible and cold flow without combustion reaction.

From the mesh independence test, the accurate total number of the grid cell is equal to 783439 cells at the TDC which it is not too low to cause a high deviation from the experimental results and it not too high that causing a long calculation time. Then, the new meshing strategy proposed in this study provides a good flexibility to generate a suitable grid for IC-

engine. In fact, the predicted results from the new proposed strategy shows an improvement of the results accuracy compared to the classical methods previously published an the anterior works. Then, the magnitude of the swirl and tumble variation change from the positive to negative values and verse versa during the intake and compression strokes. This fact indicates that the overall airflow motion changes in its direction with the crank angle. In addition, the in-cylinder pressure is taken uniform with x-position for the all z-positions and the temperature distribution of the flow increases with the increase of the crank angle.

Globally, this study proves that the cold flow analysis can be investigate the motion of the flow during the engine cycle, by visualizing the air admission at the intake stroke, and predicting the production of the swirl and the tumble ratios. Furthermore, based on the new meshing approach it is possible to manage a fine mesh with control on grid distribution for crucial zone of the geometry.

In the future, we propose to adopt this approach to study the effect of the engine load and speed on the combustion performance and emissions of a Diesel engine running with Diesel/biodiesel fuel blend.
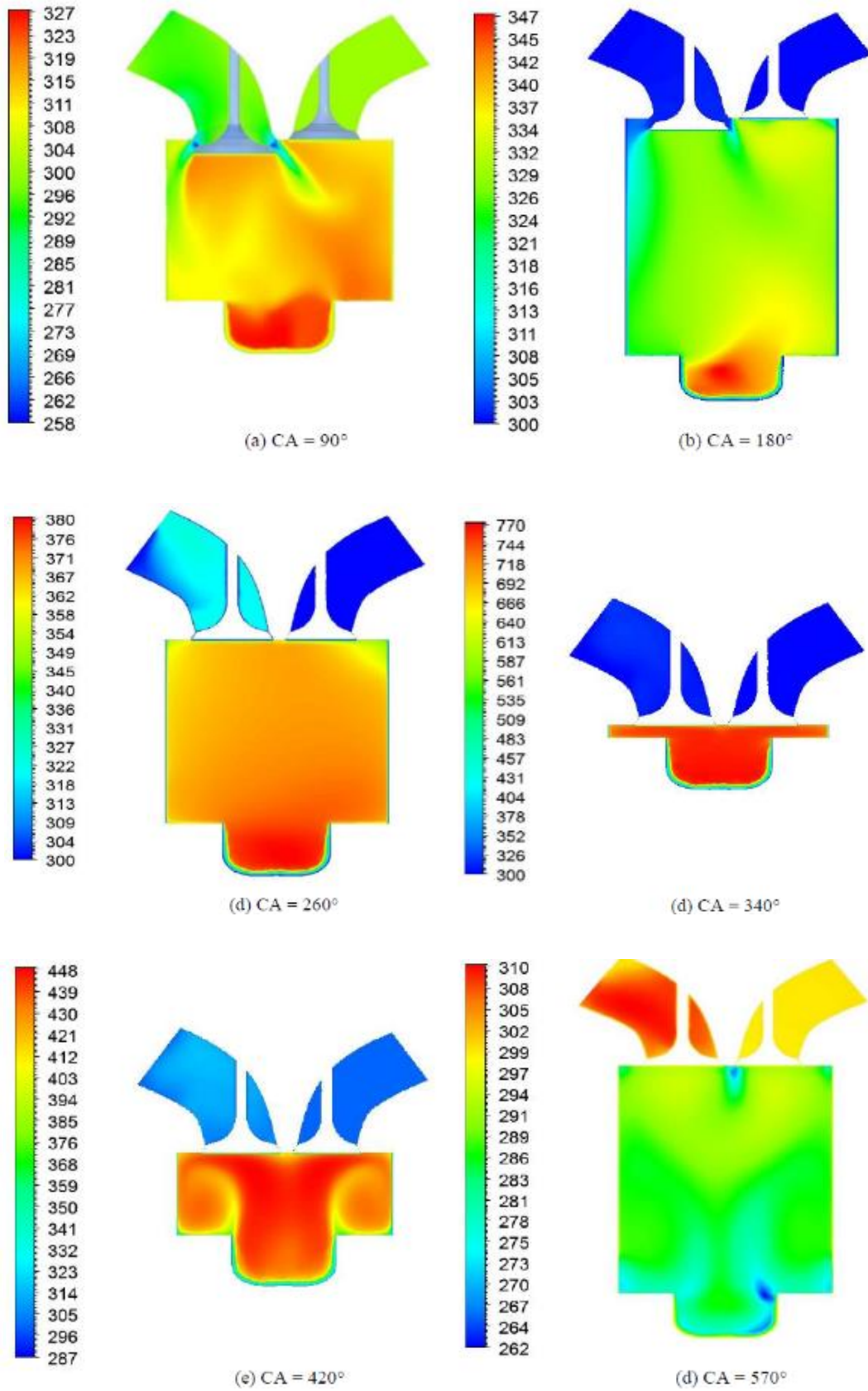
Fig. 14. In-cylinder temperature distribution.

REFERENCES

Akar, R. (2005). *Combustion chamber design with computational fluid dynamic*. National Institute of Applied Science, MSc Thesis.

Ansys ICEM CFD Tutorial manual, Ansys 17.0 help viewer.

Arcoumanis, C., A. F. Bicen and J. H. Whitelaw (1982). Measurement in a motored four stroke reciprocating model engine. *Journal of Fluids Engineering* 104-235.

Barbouchi, Z. and J. Bessrour (2009). Turbulence study in the internal combustion engine. *Journal of Engineering and Technology Research* 1 (9), 194-202.

Bilgin, A. (1999). Numerical simulation of the cold flow in an axisymmetric non-compressing engine-like geometry. *International Journal of Energy Research* 23, 899–908.

Desantes, J. M., J. V. Pastor and A. Doudou (2001). Study of the steady flow produced by direct injection Diesel engine intake ports, Proc IMechE, Part D. *Journal of Automobile Engineering* 215, 285–98.

Dillies, B., A. Ducamin, L. Lebrere and F. Neveu (1997). Direct injection Diesel engine simulation: a combined numerical and experimental approach from aerodynamics to combustion *SAE 970880*.

Driss, Z. and M. S. Abid (2012). Use of the Navier-Stokes Equations to Study of the Flow 435 Generated by Turbines Impellers. *Navier-Stokes Equations: Properties, Description and 436 Applications* (3), 51-138.

Gazeaux, J. and D. G. Thomas (2001). Caractérisation du mouvement de rotation de l'air en écoulement stationnaire dans un monocylindre Diesel en fonction des conditions d'admission. n°: 234,pp 13- 19.

Gosman, A. D., Y. Y. Tsui and A. P. Watkins (1984). Calculation of three dimensional air motion in model engines. *SAE* , 840229.

Hadj Kacem, S., M. A. Jemni, Z. Driss and M. S. Abid (2016). The effect of H2 enrichment on in-cylinder flow behavior, engine performances and exhaust emissions: Case of LPG-hydrogen Engine. *Applied Energy* 179, 961–971.

Hedfi, H., A. Jbara, H. Jedli, K. Slimi and A. Stoppato (2016). Performance enhancement of a spark ignition engine fed by different fuel types. *Energy Conversion and Management* (112), 166–175.

Hedfi, H., A. Jbara, H. Jedli and K. Slimi (2014). Modeling of a bioethanol combustion engine under different operating conditions. *Energy Conversion and Management* (88), 808–820.

Henriot, S., J. F. Le Coz and P. Pinchon (1989). Three dimensional modeling of flow and turbulence in a four-valve spark ignition engine Comparison with LDV measurements. *SAE* 890843.

Heywood, J. B. (1987). Fluid motion within the cylinder of internal combustion engines. *ASME, Journal of Fluids Engineering* 109, 3-35.

Huang, R. F., C. W. Huang, S. B. Chang, H. S. Yang, T. Lin and W. Y. Hsu (2005). Topological flow evolutions in cylinder of a motored engine during intake and compression strokes. *Fluids Struc* 20, 105–127.

Internal Combustion Engines in Workbench, Ansys Tutorials 15.0 (2013).

Jameel Basha, S. M. (2009). Simulation of in-cylinder processes in a di diesel engine with various injection timings. *ARPN Journal Of Engineering and Applied Sciences* 4, 1-7.

Jayashankara, B. and V. Ganesan (2010). Effect of fuel injection timing and intake pressure on the performance of a DI diesel engine – A parametric study using CFD. *Energy Conversion and Management* 51, 1835–1848.

Johan, Z., A. C. M. Moraes, J. C. Buell and R. M. Ferencz (2001). In-cylinder cold flow simulation using a finite element method. *Computer Methods in Applied Mechanics and Engineering* 190, 3069–3080.

Kampanis, N., C. Arcoumanis, R. Kato and S. Kometani (2001). Flow, Combustion and Emissions in a Five-Valve Research Gasoline Engine. *SAE Technical Papers Series*. No. 01-3556.

Kang, K. Y. and J. H. Baek (1998). Turbulence characteristics of tumble flow in a four-valve Engine. *Experimental Thermal and Fluid Science* 18, 231– 243.

Kim, J. N., H. Y. Kim, S. S. Yoon, J. H. Sohn and C. R. Kim (2009). Numerical studies on the mixing characteristics of exhaust gas recirculation gases with air, and their dependence on system geometries in four-cylinder engine applications, Proc IMechE, Part D. *Journal of Automobile Engineering* 223, 585.

Launder, B. E. and D. B. Spalding (1986). The numerical computation of turbulent flows. *Computer Methods in Applied Mechanics and Engineering* 3, 267-289.

Mehta, P. S. and T. Bhaskar (2001). Prediction of combustion and in-cylinder emissions in a direct injection diesel engine using multi-process models. *In: The 5th international symposium on diagnostics and modeling of combustion in IC engines,* COMODIA.

Moussa, O. and Z. Driss (2017). Numerical Investigation of the Turbulence Models Effect on the Combustion Characteristics in a Non-Premixed Turbulent Flame Methane-Air. *American Journal of Energy Research* 5, 3, 85-93.

O'Connor, J. and M. Musculus (2013). Effects of exhaust gas recirculation and load on soot in a heavy-duty optical diesel engine with close-coupled post injections for high-efficiency combustion phasing. *International Journal of Engine Research* 0(0), 1–23.

Payri, F. J., X. Benajes and A. Margot (2004). Gil CFD modeling of the in-cylinder flow in direct-injection Diesel engines. *Computers & Fluids* 33, 995–1021.

Payri, F., J. M. Desantes and J. V. Pastor (1996). LDV measurements of the flow inside the combustion chamber of a 4-valve D.I. Diesel engine with axisymmetric piston bowls. *Experiments in Fluids* 22, 118–28.

Reeves, M., D. P. Towers, B. Tavender and C.H. Buckberry (1999). A High Speed All-Digital Technique for Cycle-Resolved 2-D Flow Measurement and Flow Visualization within SI Engine Cylinders. *Journal of Optics and Laser in Engineering* 31, 247-261.

Song, J., C. Yao, Y. Liu and Z. Jiang (2008). Investigation on flow field in simplified piston bowls for DI diesel engine. Engineering Applications of Computational Fluid Mechanics 2, 354–365.

Sukegawa, Y., T. Nogi and Y. Kihara (2003). In-Cylinder Airflow of Automotive Engine by Quasi-Direct Numerical Simulation. *Journal of JSAE Review* 24, 123-126.

Sushma, H. and K. B. Jagadeesha (2013). CFD modeling of the in-cylinder flow in direct-injection diesel engine. *International Journal of Scientific and Research Publications* 3(12), 2250-3153.

Varol, Y., H. F. Oztop, M. Firat and A. Koca (2010). CFD modeling of heat transfer and fluid flow inside a pent-roof type combustion chamber using dynamic model. *International Communications in Heat and Mass Transfer* 37, 1366–1375.

Yun, J. E. New evaluation indices for bulk motion of in-cylinder flow through intake port system in cylinder head, Proc IMechE, Part D: *Journal of Automobile Engineering* 13- 21.